Naringenin modulates the NO-cGMP-PKG signaling pathway by binding to AKT to enhance osteogenic differentiation in hPDLSCs

SHENGHONG LI[1,2], ZHENQIANG XIONG[1,2], YUXIN LAN[1,2], QIAN ZHENG[1,2], LI ZHANG[1,2] and XIAOMEI XU[1-3]

[1]Department of Orthodontics, The Affiliated Stomatology Hospital, Southwest Medical University, Luzhou, Sichuan 646000, P.R. China; [2]Luzhou Key Laboratory of Oral and Maxillofacial Reconstruction and Regeneration, The Affiliated Stomatology Hospital, Southwest Medical University, Luzhou, Sichuan 646000, P.R. China; [3]Institute of Stomatology, Southwest Medical University, Luzhou, Sichuan 646000, P.R. China

Received January 23, 2024; Accepted May 22, 2024

DOI: 10.3892/ijmm.2024.5391

Abstract. Naringenin (NAR) is a prominent flavanone that has been recognized for its capacity to promote the osteogenic differentiation of human periodontal ligament stem cells (hPDLSCs). The present study aimed to explore how NAR promotes the osteogenic differentiation of hPDLSCs and to assess its efficacy in repairing alveolar bone defects. For this purpose, a protein-protein interaction network of NAR action was established by mRNA sequencing and network pharmacological analysis. Gene and protein expression levels were evaluated by reverse transcription-quantitative and western blotting. Alizarin red and alkaline phosphatase staining were also employed to observe the osteogenic capacity of hPDLSCs, and immunofluorescence was used to examine the co-localization of NAR molecular probes and AKT in cells. The repair of mandibular defects was assessed by micro-computed tomography (micro-CT), Masson staining and immunofluorescence. Additionally, computer simulation docking software was utilized to determine the binding affinity of NAR to the target protein, AKT. The results demonstrated that activation of the nitric oxide (NO)-cyclic guanosine monophosphate (cGMP)-protein kinase G (PKG) signaling pathway could promote the osteogenic differentiation of hPDLSCs. Inhibition of AKT, endothelial nitric oxide synthase and soluble guanylate cyclase individually attenuated the ability of NAR to promote the osteogenic differentiation of hPDLSCs. Micro-CT and Masson staining revealed that the NAR gavage group exhibited more new bone formation at the defect site. Immunofluorescence assays confirmed the upregulated expression of Runt-related transcription factor 2 and osteopontin in the NAR gavage group. In conclusion, the results of the present study suggested that NAR promotes the osteogenic differentiation of hPDLSCs by activating the NO-cGMP-PKG signaling pathway through its binding to AKT.

Correspondence to: Professor Xiaomei Xu, Department of Orthodontics, The Affiliated Stomatology Hospital, Southwest Medical University, 10 Yunfeng Road, Luzhou, Sichuan 646000, P.R. China
E-mail: xuxiaomei@swmu.edu.cn

Key words: naringenin, AKT, periodontal ligament stem cells, osteogenic differentiation, nitric oxide-cyclic guanosine monophosphate-protein kinase G signaling axis

Introduction

Maxillofacial trauma is increasing on a global scale (1), which poses challenges in regenerating jaw tissue and fixing alveolar bone defects. However, the potential of stem cell technology for facilitating tissue regeneration and reconstruction has emerged (2). Notably, periodontal stem cells have been identified as ideal seed cells for tissue regeneration, which is attributed to their robust proliferation and versatile differentiation capabilities (3,4). Over the years, extensive efforts have been undertaken to unravel the optimal conditions for osteogenic differentiation of human periodontal ligament stem cells (hPDLSCs), and previous research has revealed the pivotal role of the external microenvironment in influencing stem cell differentiation towards specific cell types (5).

Naringenin (NAR) is abundant in citrus, grape and tomato (6), and holds notable research and development potential. Specifically, various studies have indicated its anti-inflammatory and antioxidant capacities (7,8) and its role in conditions such as tumors, cancer and hyperlipidemia (9). However, there is limited research on the impact of NAR on bone metabolism. Kaczmarczyk-Sedlak *et al* (10) and Gera *et al* (11) observed improved osteoporosis symptoms in rats treated with NAR. A previous study also demonstrated the ability of NAR to effectively enhance the osteogenic differentiation of hPDLSCs (12). Despite these findings, the precise mechanism underlying the promotion of osteogenic differentiation of hPDLSCs by NAR remains unclear.

In the past, the exploration of new drugs and the detection of drug targets involved extensive, time-consuming and costly experiments (13). However, recent advancements in biomolecular technology have offered more possibilities for modern medical research. The development of multi-omics technology, morphology and physiology has enabled the explanation of entire biological systems and their activities (14).

Simultaneously, the rapid progress in network pharmacology (15) has made the prediction of drug action targets possible. Integrating network pharmacology with multi-omics facilitates a comprehensive understanding of drug effects on biological systems in a multi-dimensional, multi-level mechanistical manner. This approach offers new perspectives on unraveling the intricate principles of Traditional Chinese Medicine and provides more evidence for its application (16). Consequently, the present study aimed to explore the target and mechanism of NAR in promoting the osteogenic differentiation of hPDLSCs using mRNA sequencing, network pharmacology and experimental validation.

Materials and methods

Cell culture and differentiation. The present study was approved by the Ethics Committee of The Affiliated Stomatology Hospital, Southwest Medical University (Luzhou, China; approval no. 20221107003). Premolar teeth were extracted for orthodontic reasons, and written consent was provided by the guardian and patient for the use of these teeth in the present research project. In total, 34 premolars were collected from patients (12-14 years old) from November to December, 2022 at The Affiliated Stomatology Hospital, Southwest Medical University. PBS containing 5, 2 and 1% streptomycin/penicillin were prepared and used for washing roots, while the periodontal membrane was delicately removed from the middle 1/3 of the roots. The periodontal ligament tissue was seeded in a culture flask with 2 ml complete medium, which contained 89% a MEM medium (Gibco; Thermo Fisher Scientific, Inc.), 10% fetal bovine serum (Procell Life Science & Technology Co., Ltd.) and 1% streptomycin/penicillin (Beyotime Biotechnology Co., Ltd.). The flask was placed inverted in an incubator at 37˚C (5% CO_2). After 2-3 h, the cell culture flask was inverted. Third-generation cells were collected for adipogenic and osteogenic induction. The medium was changed to either osteogenic medium [complete medium with 50 μg/ml ascorbic acid (Beyotime Biotechnology Co., Ltd.), 100 nmol/l dexamethasone (Beijing Solarbio Science & Technology Co., Ltd.) and 10 mmol/l β-glycerophosphate (Beijing Solarbio Science & Technology Co., Ltd.)] or adipogenic induction medium [complete medium with 100 μmol/l indomethacin (Beijing Solarbio Science & Technology Co., Ltd.), 0.5 mmol/l 3-isobutyl-1-methyl xanthine (Beijing Solarbio Science & Technology Co., Ltd.), 10 μg/ml insulin (Beyotime Biotechnology Co., Ltd.) and 1 μmol/l dexamethasone (Beijing Solarbio Science & Technology Co., Ltd.)] and refreshed every 3 days. Alizarin red S staining (2%) for calcified nodules (37˚C, 1 h) was performed after 28 days, while oil red O staining (0.3%) for fat droplet (37˚C, 30 min) was conducted after 21 days.

Flow cytometry. Surface markers for the third-generation hPDLSCs were identified by flow cytometry. Cells were resuspended in 1-2 ml PBS and placed into assay tubes. Flow cytometry assay-associated surface marker antibodies (BD Biosciences), including CD31 (cat. no. 560984; FITC), CD44 (cat. no. 561858; PE), CD45 (cat. no. 560976; FITC), CD105 (cat. no. 560839; PE) and CD90 (cat. no. 555596; PE), were pre-diluted for use at the recommended volume per test. These antibodies were added to the cells and incubated at 4˚C for 30 min in the dark. Subsequently, the cells were washed with PBS thrice, resuspended in PBS and subjected to flow cytometry using a BD FACS Calibur (BD Biosciences). Evaluation and analysis of stem cell characteristics were conducted by detecting the specific stem cell surface markers CD31, CD44, CD45, CD90 and CD105. The results were analyzed by BD CellQuest Pro software 5.1 (BD Biosciences).

Cell treatment. Cells treated with NAR (10 μmol/l) were also treated with NG-nitro-L-arginine methyl ester (L-NAME; 70 μM) to inhibit endothelial nitric oxide synthase (eNOS), 1H-[1,2,4]oxadiazolo[4,3-a]quinoxalin-1-one (ODQ; 20 μM) to inhibit soluble guanylate cyclase (sGC) and AKT inhibitor VIII (58 nM) to inhibit AKT, as recommended by the manufacturer (MedChemExpress for all).

Cytotoxicity analysis. The third-generation hPDLSCs were seeded at a density of $5x10^3$ cells per well in 96-well plates, and the impact of 10 μmol/l NAR on the viability of hPDLSCs was assessed. After 7 days, the absorbance at 450 nm was measured with a plate reader (Thermo Fisher Scientific, Inc.) following the instructions provided by the manufacturer of Cell Counting Kit-8 (37˚C, 1 h; APeXBIO Technology LLC).

Detection of protein expression by western blotting. After 7 days of culture, cells subjected to different treatments were washed with PBS and lysed by RIPA lysis buffer (cat. no. PC101; Shanghai Epizyme Biotech Co., Ltd.) containing protease (cat. no. GRF101; Shanghai Epizyme Biotech Co., Ltd.) and phosphatase inhibitors (cat. no. GRF102; Shanghai Epizyme Biotech Co., Ltd.; 1:100). The BCA protein assay kit was used to determine the concentration of proteins. After the addition of 5X SDS-PAGE protein loading buffer, the samples underwent a 10-min incubation in a metal water bath at 100˚C. Subsequently, 20 μg protein per lane was subjected to 6, 7.5 or 10% SDS-PAGE, then transferred onto PVDF membranes. After blocking (room temperature, 10 min) by Protein Free Rapid Sealing Solution (cat. no. PS108P; Shanghai Epizyme Biotech Co., Ltd.), the membranes were incubated with 1:2,000 diluted primary antibodies (ImmunoWay Biotechnology Company) against Runt-related transcription factor 2 (RUNX2; cat. no. YT5356), osteopontin (OPN; cat. no. YT3467), sGC (cat. no. YN5360), protein kinase G (PKG; cat. no. YN1879), transient receptor potential cation channel, subfamily C, member 6 (TRPC6; cat. no. YN4084), AKT (cat. no. YT0185), phosphorylated (p)-AKT (cat. no. YP0006), eNOS (cat. no. YT3174), p-eNOS (cat. no. YP0514) and GAPDH (cat. no. YN5585) for 24 h at 4˚C, followed by a 1-h incubation with the Goat Anti-Rabbit IgG H&L antibody (Beijing Biosynthesis Biotechnology Co., Ltd.; cat. no. YP0514; 1:3,000) at room temperature. Protein bands were developed by Omni-ECL™ Femto Light Chemiluminescence kit (cat. no. SQ201; Shanghai Epizyme Biotech Co., Ltd.) after immersion of the membrane in the developing solution. GAPDH served as an internal reference to calculate the relative expression of other target proteins by ImageJ (version 1.52; National Institutes of Health).

Table I. Primer sequences.

Gene	Forward primer, 5'-3'	Reverse primer, 5'-3'
GAPDH	GCACCGTCAAGGCTGAGAAC	TGGTGAAGACGCCAGTGGA
RUNX2	CCCAGTATGAGAGTAGGTGTCC	GGGTAAGACTGGGTCATAGGACC
OPN	GATGGCCTTGTATGCACCATTC	GCAGACCTGACATCCAGTACC
sGC	GACCGATTCAGATGAGGATAGGA	GGTAAGTGGTTGGGCTGACA
PKG	AACGAGCTGGGACAAGTACCG	GATCCTTGGACTGGTGGGCTC
TRPC6	AAGACATCTTCAAGTTCATGGTC	TCAGCGTCATCCTCAATTTCC

RUNX2, Runt-related transcription factor; OPN, osteopontin; sGC, soluble guanylate cyclase; PKG, protein kinase G; TRPC6, transient receptor potential cation channel, subfamily C, member 6.

Reverse transcription-quantitative PCR (RT-qPCR). After 7 days of incubation, total RNA extraction was performed with Rapid RNA Extraction kit (Hunan Accurate Bio-Medical Technology Co., Ltd.), and RNA was reverse transcribed using Reverse Transcription Premix Kit according to the manufacturer's protocol (Hunan Accurate Bio-Medical Technology Co., Ltd.). The primer sequences for qPCR are listed in Table I. The primers (Sangon Biotech Co., Ltd.) SYBR (Hunan Accurate Bio-Medical Technology Co., Ltd.) and cDNA were added in octuplet tubes and qPCR was performed following a preset program (step 1: 95˚C, 30 sec, 1 cycle; step 2: 95˚C, 5 sec, 40 cycles; step 3: 60˚C, 30 sec, 40 cycles) (Bio-Rad Laboratories, Inc.). Gene expression was normalized to GAPDH, which served as an internal reference. The $2^{-\Delta\Delta Cq}$ method was used for data analysis (17).

Alkaline phosphatase (ALP) staining. After 7 days of incubation at 37˚C, cells from different treatment groups were washed with PBS thrice then fixed with 4% paraformaldehyde for 30 min at room temperature. The cells were then incubated with freshly prepared ALP staining reagent (Sangon Biotech Co., Ltd.) at 37˚C for 30 min. Subsequently, ALP staining was observed and recorded by light microscopes and cameras.

Alizarin red staining. Following 28 days of incubation, cells from various treatment groups were washed with PBS thrice and subsequently fixed with 4% paraformaldehyde for 30 min at room temperature. Next, cells underwent 2-3 washes with 2-3 ml double-distilled water. Finally, 1 ml alizarin red dye (Beijing Solarbio Science & Technology Co., Ltd.) was added to each well, and the cells were incubated for 30 min at 37˚C in an incubator. The wells were then washed thoroughly with double-distilled water, and the mineralized nodules were observed and recorded by light microscopes and cameras.

Molecular docking. The three-dimensional (3D) structure of the AKT receptor protein (ID: 1UNQ) was downloaded from the Research Collaboratory for Structural Bioinformatics Protein Data Bank (PDB) database (https://www.rcsb.org/). Additionally, the PubChem database (https://pubchem.ncbi.nlm.nih.gov/) was queried for NAR (compound CID: 932), and the molecular ligand 3D structure was retrieved and downloaded. Subsequently, both the AKT protein and NAR molecular files were converted to a PDBQT format, which involved the elimination of all water molecules and the addition of polar hydrogen atoms. Molecular docking was then conducted by using Autodock 4.2 (18) and Autodock Vina 1.2.2 (19), and these tools were employed to calculate the binding energy between AKT and NAR. The visualization of the final docking results was performed using Ligplot v.2.2.4 (EMBL-EBI) and Pymol 2.4.0 (Schrödinger, Inc.).

Quantitative detection of differentially expressed genes and correlation analysis. The high-throughput sequencing service and subsequent bioinformatics analysis were provided by Novogene Co. Ltd. (Beijing, China). Briefly, after 7 days of culture, total RNA was extracted by TRIzol (Thermo Fisher Scientific, Inc.) from the cells of various treatment groups. Subsequently, the gene expression of both the control and experimental groups was assessed, the differentially expressed mRNAs (GEO ID: GSE266150) were identified by Novogene Co. Ltd., with the value of |log2FoldChange|>1 and Padj <0.01. This was followed by Kyoto Encyclopedia of Genes and Genomes (KEGG) enrichment analysis, which characterized the functional pathways associated with the differentially expressed genes.

Protein-Protein Interaction (PPI) network. The key genes involved in the cGMP-PKG signaling pathway were identified using the KEGG database online tool (https://www.genome.jp/kegg/). The NAR target gene set was obtained through the Encyclopedia of Traditional Chinese (20) database (http://www.tcmip.cn/ETCM/index.php/Home/Index/index.html). These two gene sets were entered into the STRING database (https://cn.string-db.org/) to generate the PPI network. The network was analyzed using Cytoscape 3.9.1 (https://cytoscape.org/) and the genes were ranked after calculating the score of each gene. The top ten ranked genes were selected to construct the core sub-network.

cGMP ELISA. The cGMP ELISA was conducted using the human cyclic guanosine monophosphate ELISA kit (cat. no. F2502-A; Beijing Huabodeyi Biotechnology Co., Ltd.). After a 2-day incubation, the medium from hPDLSCs from various treatment groups was collected. The cGMP standard solutions were diluted to 0.1, 0.2, 0.4, 0.8 and 1.6 nmol/l according to the provided instructions Subsequently, the samples and the standard solutions were added to a 96-well

plate and incubated at 37˚C for 30 min. After completion of the reaction between the samples or the standard solutions with the Enzyme Coating Plates, the samples and the standards were discarded. Next, the washing solution was added to the 96-well plate five times, then 50 μl enzyme labeling reaction solution was added to all wells except the blank wells. The reaction was then incubated at 37˚C for an additional 30 min. The enzyme labeling reaction solution was then discarded and the 96-well plate was washed with washing solution five times. Color rendering solution A and B were added to the 96-well plate successively, then the 96-well plate was incubated at 37˚C for 10 min without light. Subsequently, terminating solution was added to terminate the reaction. Finally, the cGMP level was quantified according to the optical density (OD) at 405 nm by comparison with the standard curves.

NO detection. NO detection was conducted using the Griess Reagent kit (cat. no. S0021S; Beyotime Biotechnology Co., Ltd.). hPDLSCs were seeded in 6-well plates at a density of $1.0x10^6$ cells per well, subjected to the various aforementioned treatments for 24 h, then the supernatant was collected. The $NaNO_2$ standard solutions with concentrations ranging from 0 to 100 μM were prepared with complete medium. Next, 50 μl standards and 50 μl samples were added separately to each well of a 96-well plate. Subsequently, NO detection reagents I and II were added (50 μl each; 37˚C, 10 min). After completion of the reaction, Finally, the resulting solutions were quantified according to the OD at 540 nm using a microplate reader (Thermo Fisher Scientific, Inc.).

Animal treatment. A total of 12 Sprague-Dawley (SD) male rats (180-220 g, 6 weeks old) purchased from Southwest Medical University Laboratory Animal Center (Luzhou, China), were divided equally into the control and NAR groups. Animals were housed in a controlled environment, including a temperature of 23±2˚C, a relative humidity of 45±5%, a 12 h light-dark cycle and access to food and water *ad libitum*. Rats were examined daily for body weight, health and behavior. Anesthesia was induced with 50 mg/kg sodium pentobarbital by intraperitoneal injection. Hair removal was achieved using depilatory cream and sequential incisions were made in the left cheek tissues. Next, a 1x1x2-mm defect was abraded underneath the molar teeth of the rats using a high-speed handpiece. After surgery, subcutaneous injection of carprofen (5 mg/kg) was used for pain relief. The NAR group received a daily gavage of 50 mg/kg NAR (Shanghai Macklin Biochemical Co., Ltd.) (21,22), while the control group received an equal volume of saline. The following conditions were set as the humane endpoints: Initial body weight loss of >20%, inability to eat and drink and animals without anesthesia or sedation showing depression or low body temperatures <37˚C. No SD rats exhibited these humane endpoints. After 28 days of continuous treatment, the SD rats were euthanized at a 50% vol/min CO_2 displacement rate (according to the AVMA guidelines) (23). After determining that the rats were not moving, not breathing and had dilated pupils, the CO_2 was switched off and the animals were observed for a further 2 min to determine that they were dead. Next, lower jaw samples were collected and then immersed in 4% paraformaldehyde (room temperature, 24 h). The animal manipulation procedures were approved by The Ethics Committee of the Laboratory Animal Center of Southwest Medical University (approval no. 20221107-016).

Masson staining and immunofluorescence. After 2-month decalcification using ethylenediaminetetraacetic acid (cat. no. ST069-500 ml; Beyotime Biotechnology Co., Ltd.), the alveolar bone tissues were embedded in paraffin and sectioned (4-μm sections), followed by Masson staining (room temperature, 2 h) (Beijing Solarbio Science & Technology Co., Ltd.) and light microscopy to observe osteogenesis at the bone defects.

For immunofluorescence staining, the tissue sections were deparaffinized with xylene (twice for 15 min each). After deparaffinization, the sections were rehydrated with different concentrations of alcohol (100, 95, 80 and 70%) and purified water. The excess water was discarded, and antigen repair was conducted by adding an appropriate amount of antigen repair solution (cat. no. P0088; Beyotime Biotechnology Co., Ltd.) to the tissues, then washing with water after 10 min. Next, the sections were blocked using 5% goat serum (Beijing Solarbio Science & Technology Co., Ltd.) for 30 min at 37˚C and then incubated overnight with anti-RUNX2 (1:100; cat. no. YT5356) and anti-OPN (1:100; cat. no. YT3467) antibodies (ImmunoWay Biotechnology Company) at 4˚C. The next day, the sections were incubated with a Multi-rAb CoraLite® Plus 594-Goat Anti-Rabbit Recombinant Secondary Antibody (1:200; cat. no. RGAR004; Proteintech Group, Inc.) at 37˚C for 1 h. Next, the sections were washed in PBS, treated with DAPI (37˚C, 10 min) and sealed with glycerol. The sections were then observed and imaged under a fluorescence microscope.

Micro-computed tomography (micro-CT). A micro-CT system (SkySCAN 1176 Micro-CT; Bruker Corporation) was employed for imaging. The imaging parameters were as follows: Pixel size=35 mm, angular rotation step=0.8 and voltage/current=50 kV/498 mA. The CT results were reconstructed, and the region of the bone corresponding to the bone defect was specifically selected for subsequent analysis. The regions of interest were analyzed using CT-Analyser (version 1.20.3.0; Bruker Corporation). The total volume of the tissue was calculated by the software by setting uniform parameters. Then, the bone mineral density (BMD), bone volume/tissue volume (BV/TV) ratio and trabecular thickness (TbTh) were assessed.

Co-localization of NAR probes and AKT. NAR probes labeled with fluorescein were synthesized through an azide-alkyne cycloaddition reaction. hPDLSCs were treated with NAR probes (10 μmol/l) and fluorescence detection was conducted after a 2-day incubation period. The treated cells were fixed using 4% paraformaldehyde (37˚C, 30 min), washed with PBS and blocked with 10% goat serum for 1 h (room temperature). The blocked cells were then incubated with anti-AKT antibody (1:100) at 4˚C overnight. The next day, the samples were incubated with a Multi-rAb CoraLite® Plus 594-Goat Anti-Rabbit Recombinant Secondary antibody (1:200; Proteintech Group, Inc.) at 37˚C for 1 h, followed by incubation with DAPI (37˚C, 10 min). The hPDLSCs were then washed with PBS thrice, sealed with glycerol and observed and imaged under a laser confocal microscope.

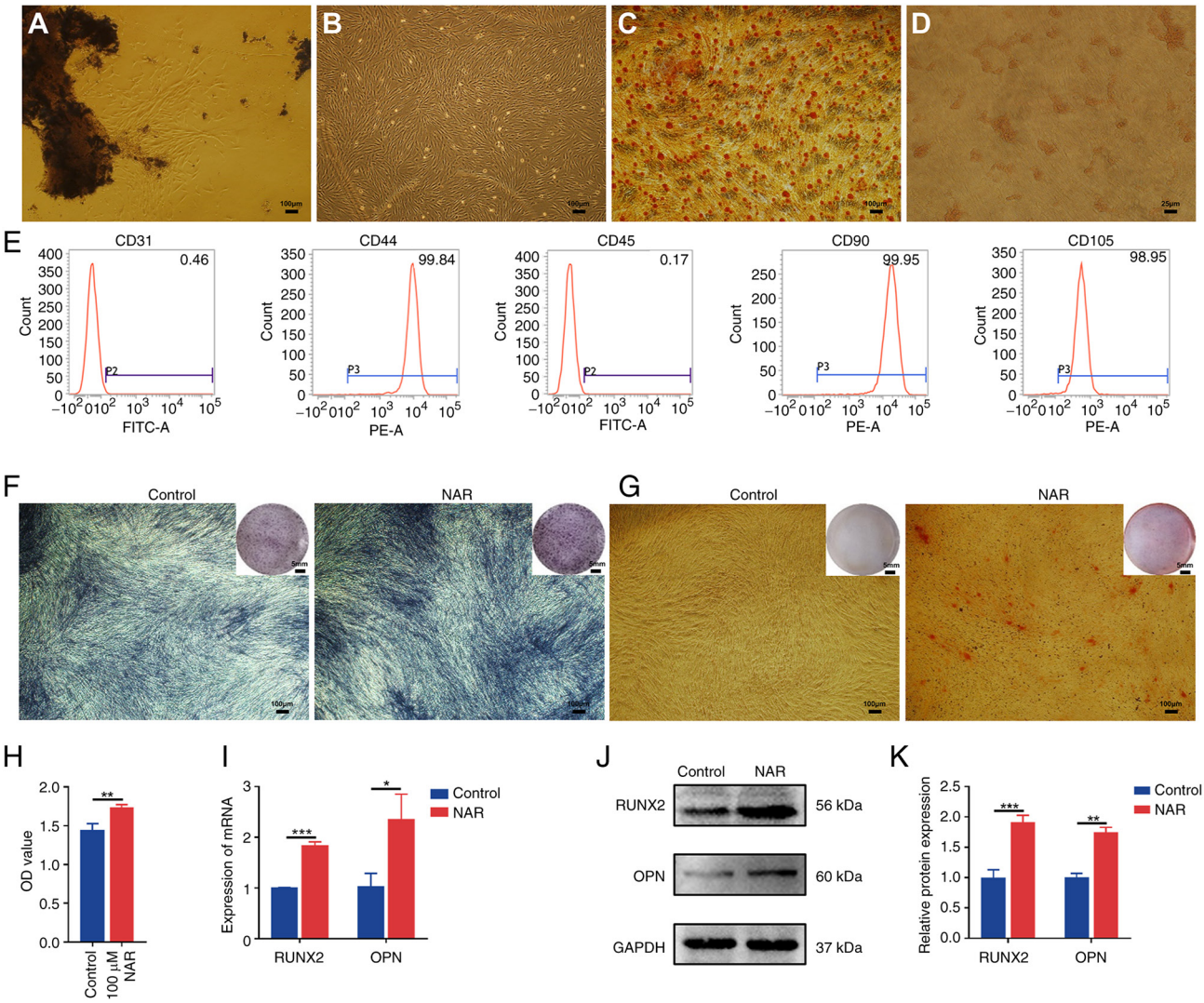

Figure 1. Isolation and identification of hPDLSCs, and NAR-mediated promotion of hPDLSC osteogenic differentiation. (A) The hPDLSCs around tissue blocks (magnification, x40). (B) The third-generation hPDLSCs (magnification, x40). (C) Alizarin red S staining demonstrating osteogenic differentiation ability of hPDLSCs (magnification, x40). (D) Oil red O staining demonstrating adipogenic differentiation ability of hPDLSCs (magnification, x200). (E) Flow cytometry results of cell surface markers. (F) Alkaline phosphatase staining of hPDLSCs after 7 days of 10 μM NAR treatment (magnification, x40). (G) hPDLSCs were subjected to alizarin red staining following incubation with NAR for 28 days (magnification, x40). (H) Results of Cell Counting Kit 8 assay. (I) Gene and (J) protein expression of RUNX2 and OPN in hPDLSCs after 7 days of 10 μM NAR treatment. (K) Histogram of RUNX2 and OPN protein expression. *P<0.05, **P<0.01, ***P<0.001. hPDLSCs, human periodontal ligament stem cells; NAR, naringenin; RUNX2, Runt-related transcription factor; OPN, osteopontin; OD, optical density.

Statistical analysis. SPSS version 21.0 (IBM Corp.) was used to analyze the data. All data are presented as the mean ± standard deviation. Statistical significance was evaluated using the Student's t-test (unpaired) for independent samples to compare the differences in the data between groups. For ≥3 groups, one-way ANOVA and Dunnett's post hoc test were employed. P<0.05 was considered to indicate a statistically significant difference.

Results

Culture and characterization of hPDLSCs. The established third-generation hPDLSCs exhibited robust osteogenic and adipogenic differentiation capabilities (Fig. 1C and D). Flow cytometry analysis confirmed the identity of hPDLSCs, which revealed positive expression of CD44 (99.84%), CD90 (99.95%) and CD105 (98.95%), and negative expression of CD31 (0.46%) and CD45 (0.17%) (Fig. 1E). Compared with the control group, hPDLSCs treated with 10 μM NAR for 7 days demonstrated enhanced osteogenic potential, as indicated by ALP staining, formation of mineralized nodules and elevated gene and protein expression of RUNX2 and OPN (Fig. 1F, G and I-K).

Volcano plots, clustered heatmaps, KEGG analysis and expression validation of genes. The transcriptome sequencing results revealed differential expression of 104 genes between the control and NAR groups (Fig. 2A and B). KEGG analysis of these differentially expressed genes revealed the involvement of the cGMP-PKG signaling pathway (Fig. 2C). The ELISA result revealed an elevated cGMP protein expression in the NAR group compared with the control group (Fig. 2D). During the assessment of pathway factors associated with the cGMP-PKG signaling axis, the NAR group was observed

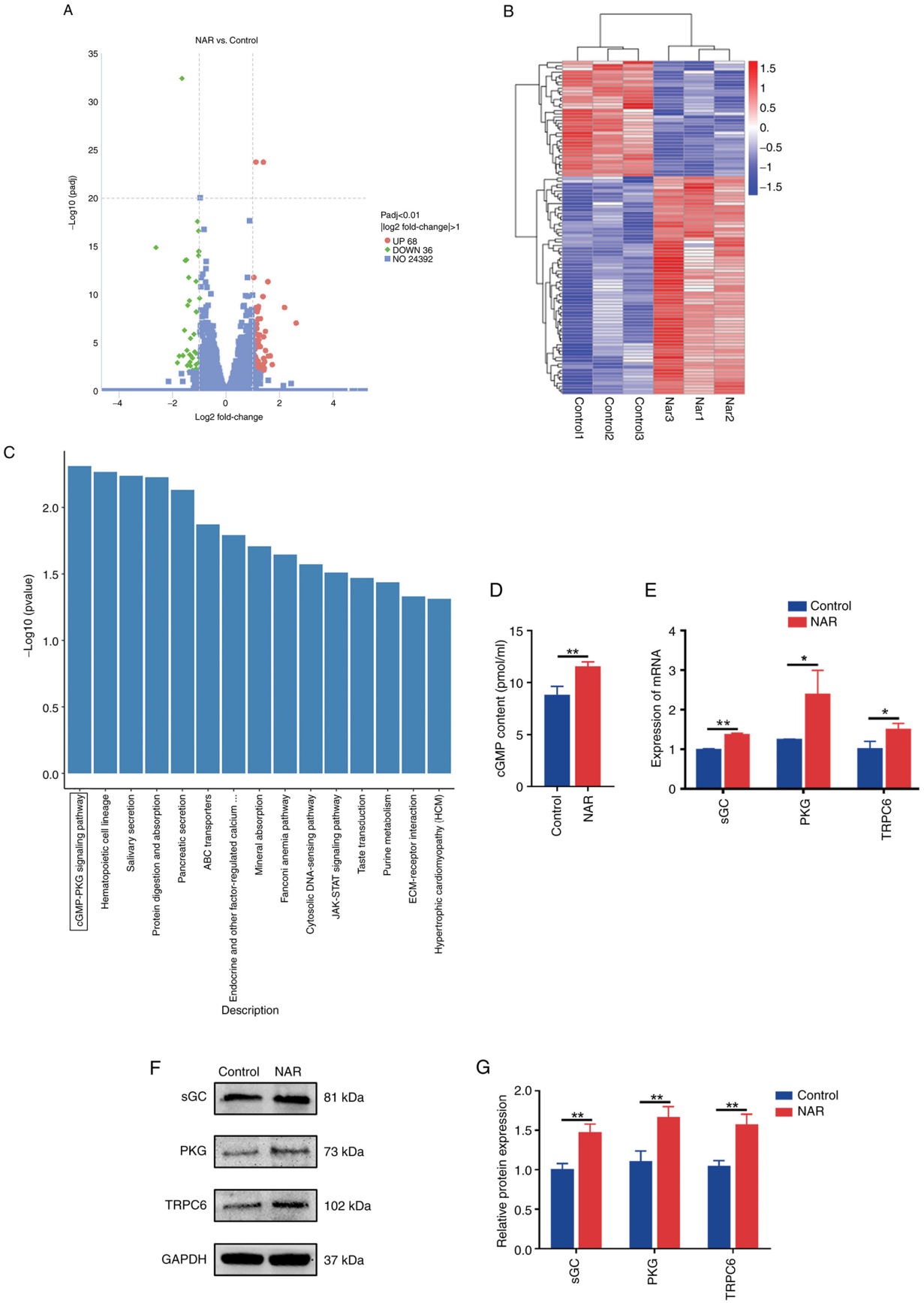

Figure 2. Volcano plot, clustered heatmap, KEGG analysis and validation of the expression of associated factors. (A) Volcano plot depicting the differential gene expression between the NAR and control groups. (B) Heatmap illustrating the gene expression differences between the NAR and control groups. (C) Kyoto Encyclopedia of Genes and Genomes analysis of differentially expressed genes between the NAR and control groups. (D) ELISA detection of cGMP production. (E) Reverse transcription-quantitative PCR-based detection of TRPC6, PKG and sGC expression. (F and G) Protein expression analysis of PKG, TRPC6 and sGC. *P<0.05, **P<0.01. NAR, naringenin; cGMP, cyclic guanosine monophosphate; TRPC6, transient receptor potential cation channel, subfamily C, member 6; PKG, protein kinase G; sGC, soluble guanylate cyclase.

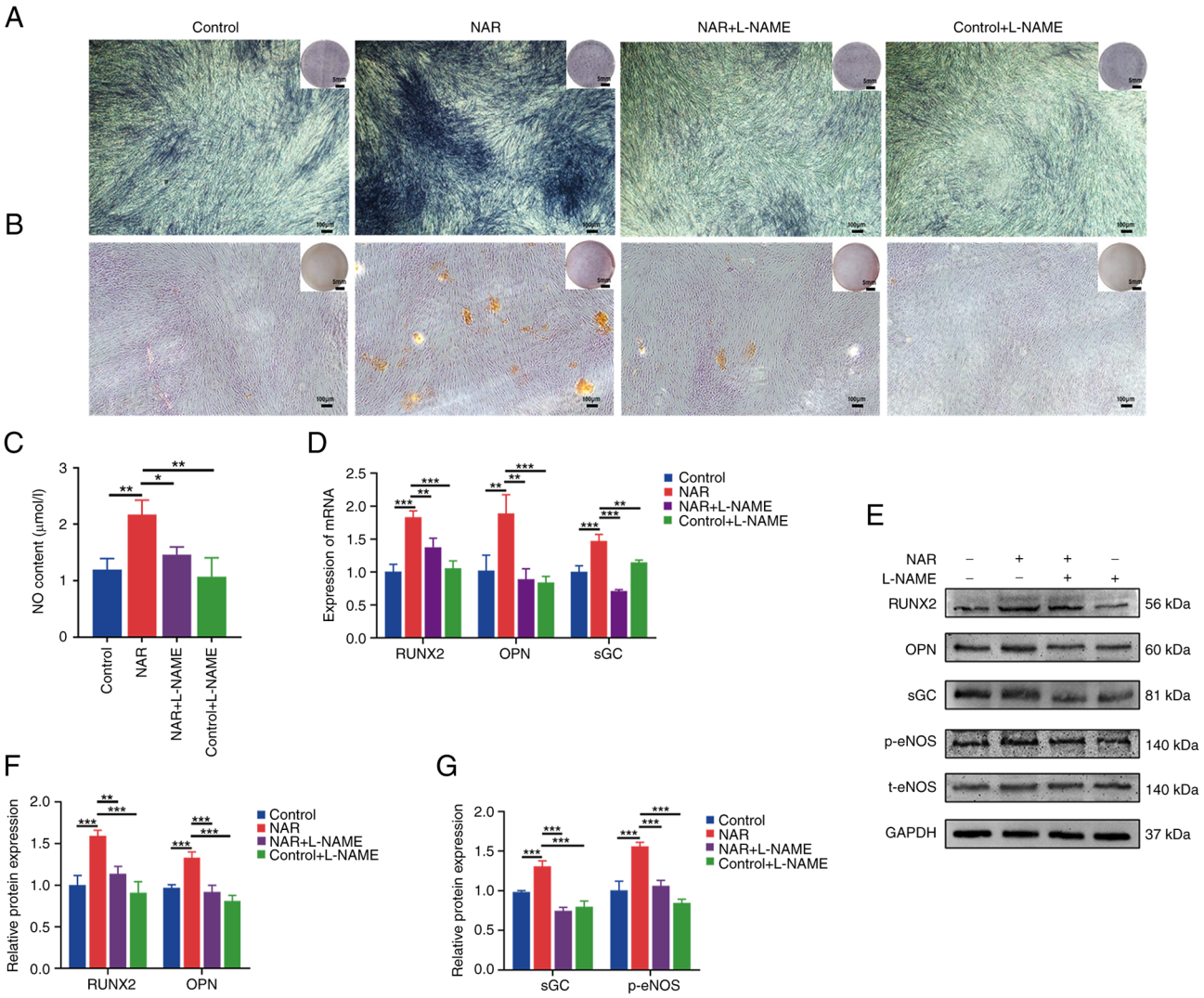

Figure 3. Ability of NAR to promote osteogenesis in human periodontal ligament stem cells is mitigated after L-NAME (eNOS inhibitor) treatment. (A) Alkaline phosphatase staining in different treatment groups. (B) Alizarin red staining in different treatment groups. (C) NO levels in different treatment groups. (D) Gene expression levels of RUNX2, OPN and sGC in different treatment groups. (E-G) Protein expression of RUNX2, OPN, sGC and p-eNOS in various treatment groups. *P<0.05, **P<0.01, ***P<0.001. NAR, naringenin; eNOS, endothelial nitric oxide synthase; RUNX2, Runt-related transcription factor; OPN, osteopontin; sGC, soluble guanylate cyclase; NO, nitric oxide; p-, phosphorylated; t-, total; L-NAME, NG-nitro-L-arginine methyl ester.

to exhibit elevated expression levels of sGC, PKG and TRPC6 proteins and genes compared with the control group (Fig. 2E-G).

Impact of the eNOS inhibitor, L-NAME, on NAR-induced promotion of osteogenic differentiation in hPDLSCs. Strong ALP and alizarin red staining was noted in the NAR group compared with the control group (Fig. 3A and B), indicating that NAR promoted the osteogenic differentiation of hPDLSCs. Additionally, the gene and protein expression levels of the osteogenesis-related factors, RUNX2 and OPN, were higher in the NAR group than in the control group (Fig. 3D-F). This elevation was accompanied by increased expression of p-eNOS, NO and sGC (Fig. 3C-E and G). Upon the addition of L-NAME (an eNOS inhibitor), the NAR + L-NAME group exhibited decreased expression of p-eNOS, NO and sGC compared with the NAR group, in addition to a decreased expression of the osteogenic factors, RUNX2 and OPN. Furthermore, the staining intensity of ALP and alizarin red was lower in the NAR + L-NAME group compared with the NAR group (Fig. 3A and B).

Ability of NAR to promote the osteogenic differentiation of hPDLSCs is decreased by the addition of ODQ, an sGC inhibitor. Further experiments were conducted to explore the role of the NO downstream factor, sGC. The results revealed an increased expression of sGC, PKG, cGMP and TRPC6 in the NAR group compared with the control group (Fig. 4C, E, F and H). Upon addition of ODQ (an sGC inhibitor), the NAR + ODQ group exhibited decreased expression of the osteogenesis-related factors, RUNX2 and OPN, at both the gene and protein levels (Fig. 4D, F and G). Additionally, the intensity of both ALP and alizarin red staining in the NAR + ODQ group was lower compared with the NAR group (Fig. 4A and B). Furthermore, the expression of sGC, PKG, cGMP and TRPC6 was reduced in the NAR + ODQ group compared with the NAR group (Fig. 4C-H).

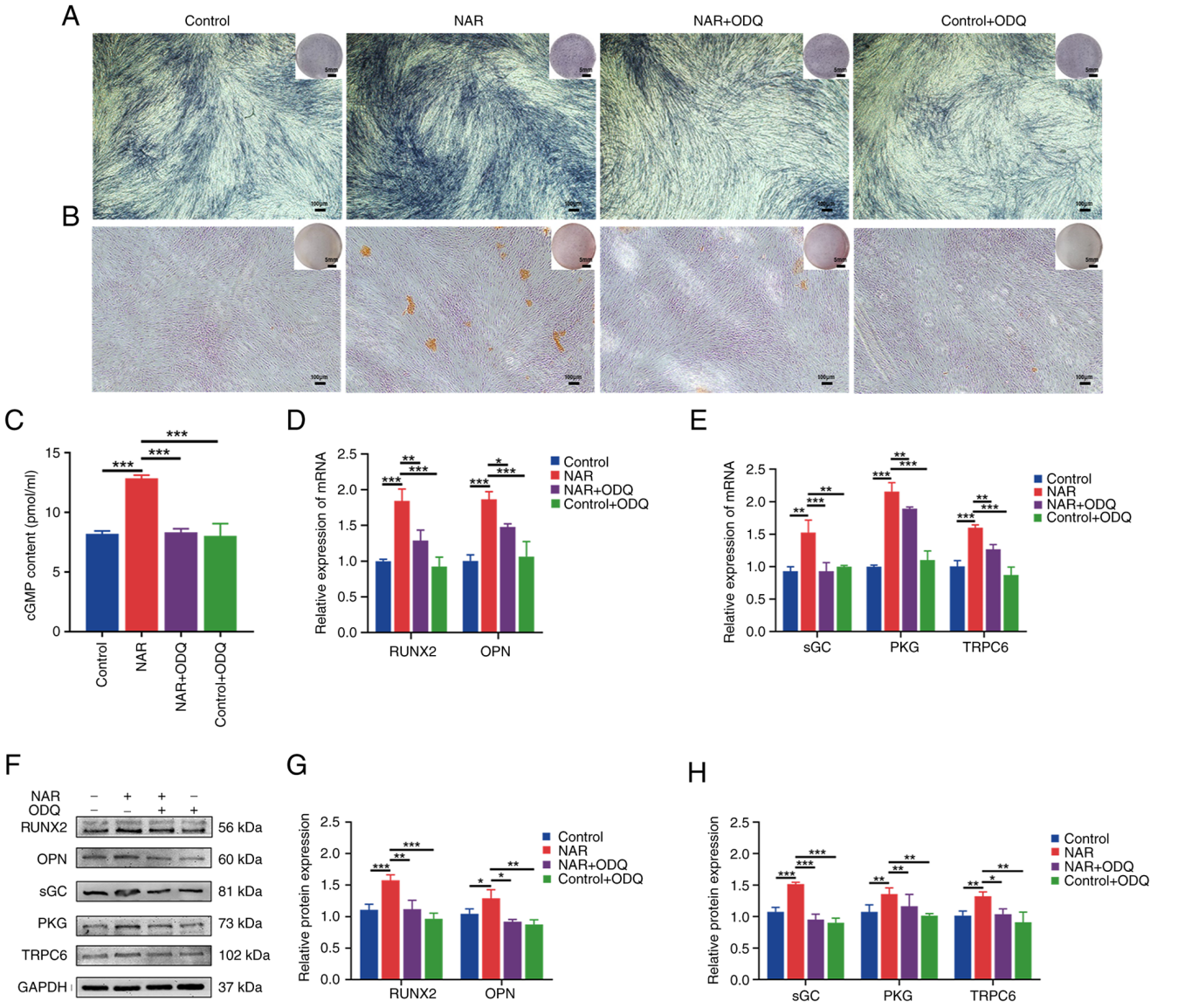

Figure 4. Ability of NAR to promote osteogenesis in human periodontal ligament stem cells is decreased after ODQ (an sGC inhibitor) treatment. (A) Alkaline phosphatase staining in different treatment groups. (B) Alizarin red staining in different treatment groups. (C) cGMP expression in different treatment groups. (D and E) Gene expression levels of RUNX2, OPN, sGC, PKG and TRPC6 in different treatment groups. (F-H) Protein levels of RUNX2, OPN, sGC, PKG and TRPC6 in different treatment groups. *P<0.05, **P<0.01, ***P<0.001. NAR, naringenin; cGMP, cyclic guanosine monophosphate; sGC, soluble guanylate cyclase; RUNX2, Runt-related transcription factor; OPN, osteopontin; TRPC6, transient receptor potential cation channel, subfamily C, member 6; PKG, protein kinase G; ODQ, 1H-[1,2,4]oxadiazolo[4,3-a]quinoxalin-1-one.

Network pharmacology screening of NAR targeting factors and validation. NO-cGMP-PKG signaling pathway-related factors and NAR targeting factors were input into the STRING database for analysis. A PPI network was generated, and the top 10 genes were used to construct the core sub-network by Cytoscape. AKT emerged as the top-ranking gene in this network, which revealed an association between AKT and eNOS (also termed NOS3; Fig. 5A). Subsequently, AKT, eNOS, NO, sGC, cGMP, PKG and TRPC6 were integrated into the cGMP-PKG signaling pathway, which revealed that AKT was situated upstream of this pathway and could directly regulate eNOS (Fig. 5B). Fig. 5C illustrates the docking results of NAR (structure downloaded from PubChem) with AKT molecules (structure downloaded from the PDB), while the 2D representation is shown in Fig. 5D. In addition, a NAR probe labeled with fluorescein was co-cultured with hPDLSCs (Fig. 5E), which revealed co-localization of the fluorescence emission of the NAR probe with that of AKT in the cytoplasm (Fig. 5F).

Ability of NAR to promote osteogenesis in hPDLSCs is decreased by the addition of AKT inhibitor VIII. The results revealed increased expression of p-AKT and p-eNOS in the NAR group compared with the control group (Fig. 6D and F). Upon addition of AKT inhibitor VIII, the NAR + AKT inhibitor VIII group exhibited decreased expression of the osteogenesis-related factors, RUNX2 and OPN, at both the gene and protein levels compared with the NAR group. Additionally, ALP and alizarin red staining exhibited a lower intensity, and the expression of p-AKT and p-eNOS was reduced in the NAR + AKT inhibitor VIII group compared with the NAR group (Fig. 6A-F).

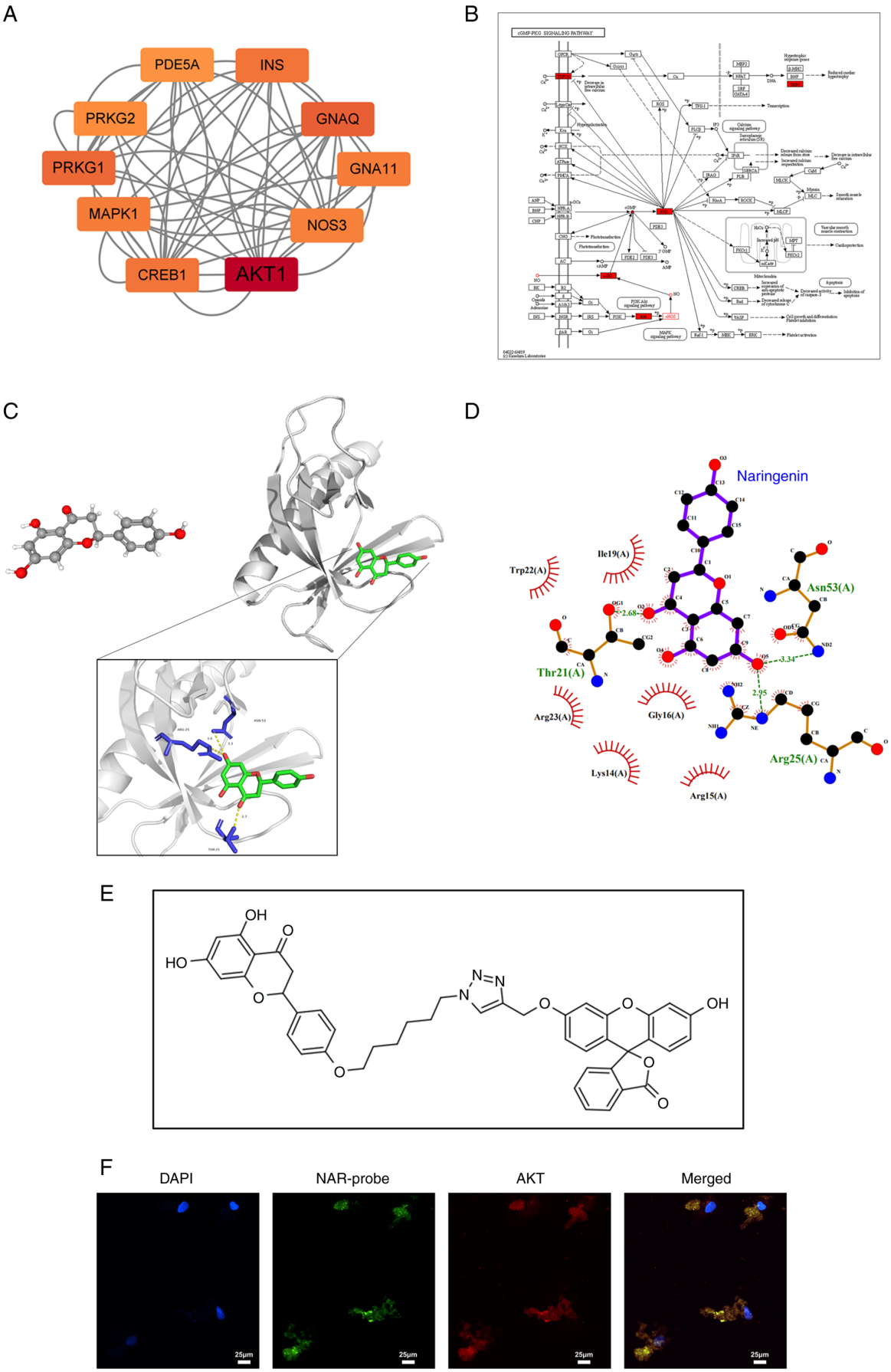

Figure 5. Network pharmacological screening and validation of NAR targeting factors. (A) Cytoscape analysis of the top 10 genes in the protein-protein interaction network. (B) Localization of crucial genes in the cyclic guanosine monophosphate-protein kinase G signaling axis. (C) 3D structure of NAR and the 3D docking results of NAR and AKT. (D) Two-dimensional docking results of NAR and AKT. (E) NAR fluorescent probe. (F) Co-localization of NAR and AKT. NAR, naringenin; 3D, three-dimensional.

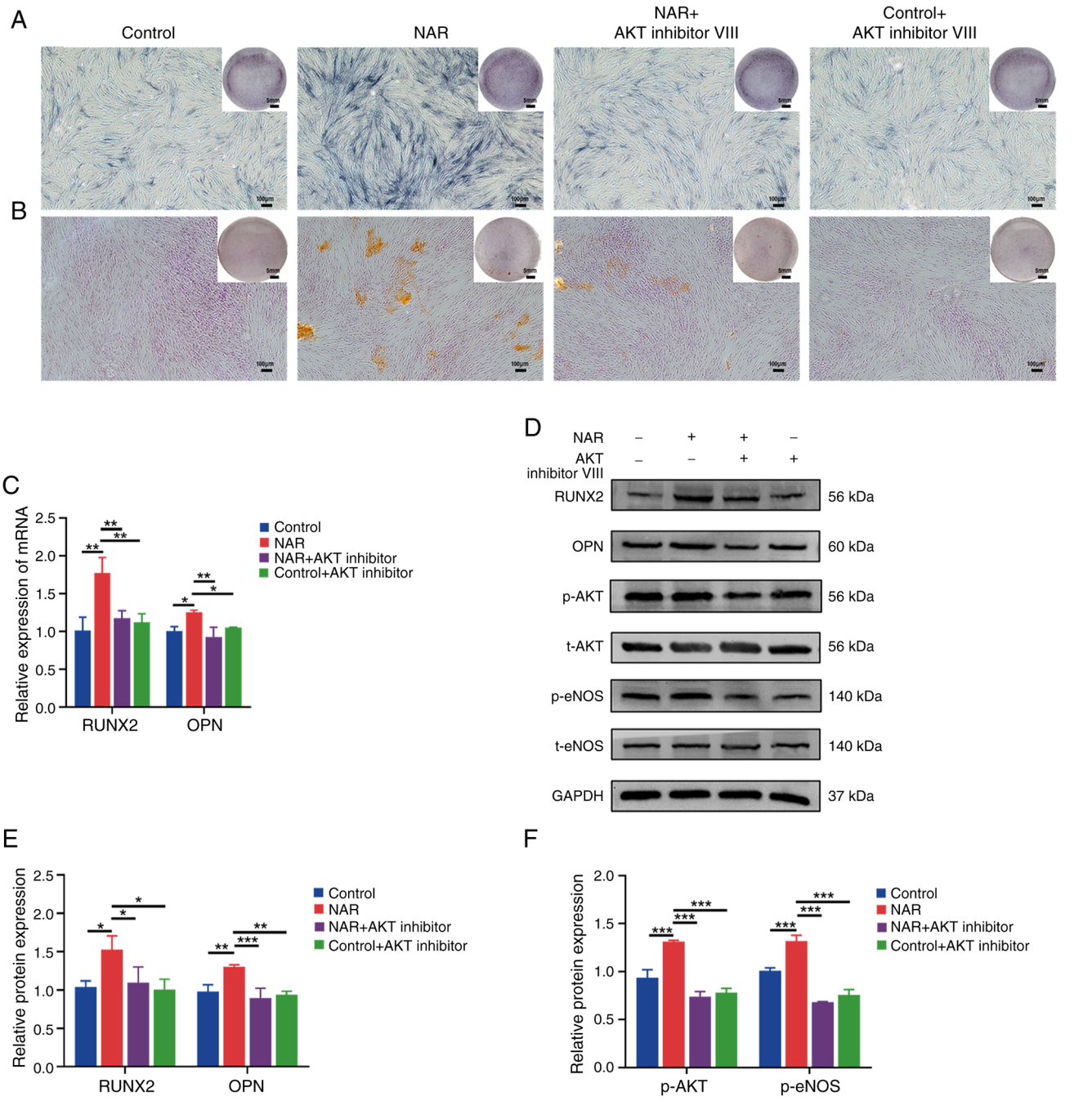

Figure 6. Impact of AKT inhibitor VIII on NAR-mediated osteogenic promotion in human periodontal ligament stem cells. (A) Alkaline phosphatase staining in different treatment groups. (B) Alizarin red staining in different treatment groups. (C) Gene expression of RUNX2 and OPN in different treatment groups. (D-F) Protein levels of RUNX2, OPN, p-AKT and p-eNOS in different treatment groups. *P<0.05, **P<0.01, ***P<0.001. NAR, naringenin; RUNX2, Runt-related transcription factor; OPN, osteopontin; eNOS, endothelial nitric oxide synthase; p-, phosphorylated; t-, total.

NAR promotes the repair of alveolar bone defects. Due to the enhanced osteogenic differentiation observed in hPDLSCs under the influence of NAR during *in vitro* experiments, it was hypothesized that NAR may promote alveolar bone regeneration. To investigate this, an alveolar bone defect model was established in SD rats, and a daily gavage of 50 mg/kg NAR was administered to the treatment group. Micro-CT analysis of bone morphology revealed that, after 28 days of treatment, new bone, BMD, BV/TV and TbTh at the bone defects were higher in the NAR group compared with the saline-treated (control) group (Fig. 7A-D). Masson staining also indicated increased formation of new bone in the NAR group (Fig. 7E). Immunofluorescence further demonstrated higher expression of RUNX2 (Fig. 7F) and OPN (Fig. 7G) in the periodontal ligament and new bone at the alveolar bone defects in the NAR group. These findings suggested that NAR has the potential to promote the healing of alveolar bone defects.

Discussion

Numerous studies have employed hPDLSCs in both *in vivo* and *in vitro* repair and regeneration experiments, demonstrating

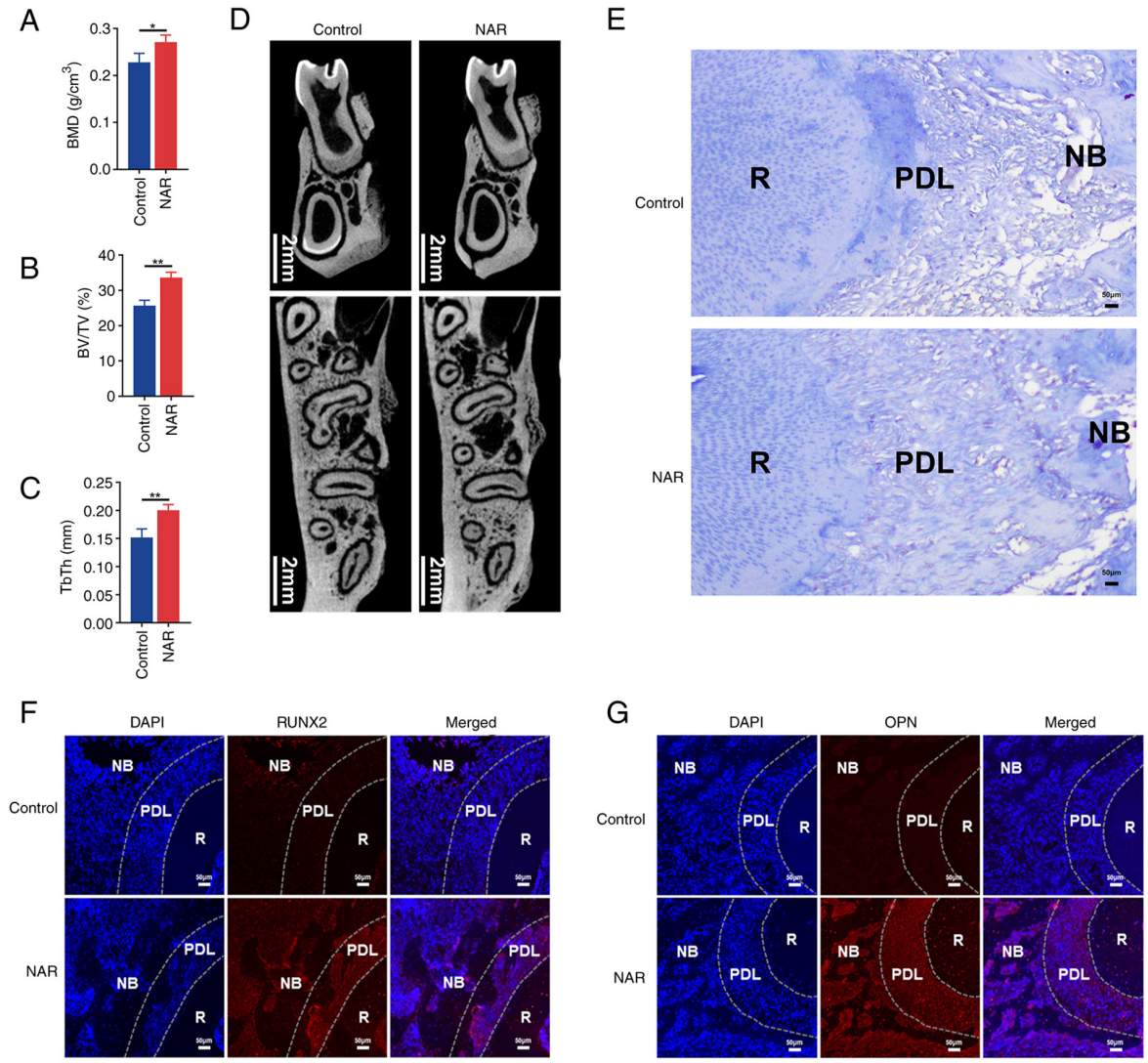

Figure 7. Ability of NAR to promote alveolar bone repair. (A-D) Results of BMD, BV/TV ratio, TbTh and new bone in the control and NAR groups. (E) Masson staining illustrating tissue morphology in the control and NAR groups. (F and G) Immunofluorescence of alveolar bone in the control and NAR groups. *P<0.05, **P<0.01. NAR, naringenin; RUNX2, Runt-related transcription factor; OPN, osteopontin; BMD, bone mineral density; BT/TV, bone volume/tissue volume; TbTh, trabecular thickness; R, root; PDL, periodontal ligament; NB, new bone.

their effectiveness in promoting osteogenesis (24-26). However, the complexity of material construction has hindered their widespread adoption. NAR holds notable development and application potential as it is readily available and easily obtainable. In the present study, bioinformatics analysis revealed the presence of differentially expressed factors in hPDLSCs after NAR treatment, and these factors were associated with the NO-cGMP-PKG signaling pathway, which is known to be involved in bone remodeling processes (27). Previous studies have suggested the promotion of osteogenic differentiation by estradiol, fluid shear stress and epimedium glycosides through the NO-cGMP-PKG signaling pathway (28-30). During the cell experiments conducted in the present study, NAR was found to enhance osteogenesis in hPDLSCs, which was accompanied by increased expression of NO and sGC, factors related to the NO-cGMP-PKG pathway.

To explore the involvement of the NO-cGMP-PKG pathway in the promotion of osteogenesis by NAR in hPDLSCs, the present study used L-NAME (an inhibitor of eNOS phosphorylation) and observed a decrease in both p-eNOS and NO expression, in addition to a decreased osteogenic capacity of hPDLSCs. These results may suggest that NO is a crucial factor in the osteogenic promotion mediated by NAR. Additionally, as a pivotal signal in bone remodeling (31), NO increases cGMP concentration and promotes osteoblast proliferation (32). The downstream factor of NO is sGC, which has been reported to further enhance osteoblast proliferation and differentiation and to reduce bone trabecular loss (33). In the present study, the addition of ODQ (an inhibitor of sGC) resulted in a decrease in the osteogenic potential of NAR-promoted hPDLSCs, which was coupled with reduced expression of downstream factors such as PKG, cGMP and TRPC6. Inhibition of TRPC6 has been shown to hinder the osteogenic capacity of periodontal ligament cells, while activation of TRPC6 promotes it. Moreover, TRPC6-knockout mice exhibit poorer bone regeneration in cranial defects compared with wild-type mice, which reflects the importance of TRPC6 in bone defect repair (34).

Beyond osteogenesis, the NO-cGMP-PKG pathway plays a role in various biological functions such as heart failure with

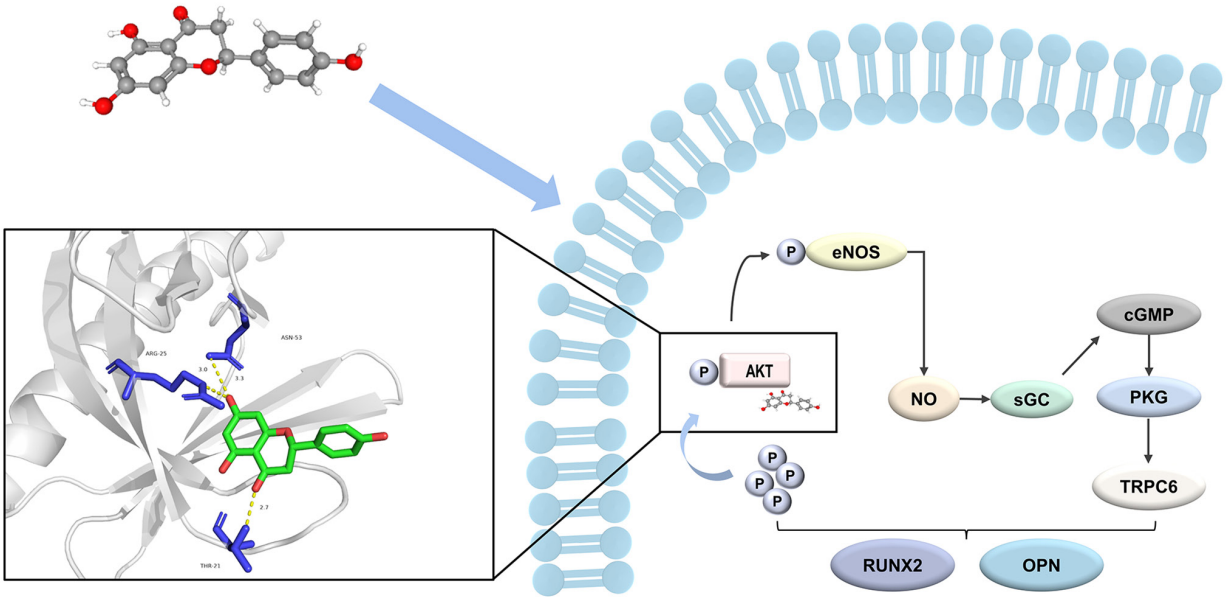

Figure 8. Schematic diagram of the mechanism by which naringenin promotes the osteogenic differentiation of human periodontal ligament stem cells. eNOS, endothelial nitric oxide synthase; p, phosphorylated; NO, nitric oxide; sGC, soluble guanylate cyclase; cGMP, cyclic guanosine monophosphate; TRPC6, transient receptor potential cation channel, subfamily C, member 6; PKG, protein kinase G.

preserved ejection fraction, gluconeogenesis and the circadian clock (35-37). NAR has been shown to reduce inflammatory pain responses induced by superoxide anion (KO_2) in mice through the NO-cGMP-PKG-ATP-sensitive potassium channel (KATP) signaling pathway (38). In addition, NAR inhibited the pacing activity of mouse small intestinal Cajal mesenchymal stromal cells through a NO-cGMP-dependent pathway (39). These findings suggest that NAR exerts diverse cellular effects by modulating the NO-cGMP-PKG pathway.

To further investigate the regulatory mechanisms by which NAR influences the NO-cGMP-PKG pathway, the present study used network pharmacology. The results of computer-simulated molecular docking revealed a strong binding affinity between NAR and AKT, which was consistent with previous studies (40-42). As indicated by pathway mapping, AKT was situated upstream of the NO-cGMP-PKG pathway. Thus, we hypothesized that NAR may activate the NO-cGMP-PKG pathway by targeting AKT. Phosphorylated AKT activates eNOS, which leads to the release of NO and subsequent protection against high glucose-induced apoptosis in endothelial cells (43). Similarly, the promotion of osteogenic differentiation in bone marrow mesenchymal stem cells by epimedium glycoside has been associated with elevated expression of p-AKT, p-eNOS and NO (30), which is in agreement with the increased expression of p-AKT and p-eNOS observed following NAR treatment of hPDLSCs in the present study. In the present study, the addition of an AKT inhibitor resulted in decreased expression of p-AKT and p-eNOS (which supported the aforementioned hypothesis) in NAR-treated hPDLSCs, which was accompanied by a reduction in the ability of NARs to promote the osteogenic differentiation of hPDLSCs.

In addition, the present study revealed that NAR bound to the R25 site on AKT, which was consistent with the binding site of SC79, a specific AKT activator that promotes the cytosolic phosphorylation of AKT (44). SC79 has been shown to contribute to the osteogenic differentiation of human bone marrow mesenchymal stem cells (45). To explore the intracellular binding of NAR to AKT, fluorescent NAR probes were synthesized and employed in the present study. The observed fluorescence co-localization of NAR with AKT confirmed that NAR may stimulate the osteogenic differentiation of hPDLSCs by intracellularly binding to AKT and promoting its phosphorylation. Previous studies have reported that NAR promotes AKT phosphorylation to regulate apoptosis and enhances the cellular cholesterol efflux process in prostate cancer cells (46,47). Notably, NAR-promoted AKT phosphorylation regulates various cellular biological functions such as inducing prostate cancer apoptosis, supporting migration of cells, improving ovulation and suppressing androgens and cystic follicles (46,48,49). In the present study, NAR gavage significantly promoted the repair and regeneration of alveolar bone defects in a bone defect model. Zhou *et al* (50) also found that NAR significantly reversed bone loss caused by LPS and contributed to the healing of cranial bone defects. These findings underscore the value of NAR in research and development for promoting bone regeneration.

However, the present study does have some limitations. Only mRNAs from transcriptomics were analyzed for relevant pathways, while transcriptomics also includes non-coding RNAs. It has previously been demonstrated that non-coding RNAs have a role in biological mechanisms (51). In the future, the functions and mechanisms of NAR and other Chinese medicine molecules should be further revealed from a multi-omics perspective.

In summary, AKT has emerged as a pivotal target through which NAR facilitates osteogenic differentiation, and the promotion of osteogenesis in hPDLSCs by NAR is achieved by binding to AKT to modulate the NO-cGMP-PKG signaling pathway (Fig. 8). The present findings constitute novel insights into the underlying mechanism by which NAR promotes the osteogenic differentiation of hPDLSCs, offering valuable knowledge for the future development and application of NAR.

Acknowledgements

Not applicable.

Funding

The present study was supported by the Sichuan Provincial Bureau of Traditional Chinese Medicine Project (grant no. 2023MS080), Innovation Project of Science and Technology Department of Sichuan Province (grant no. 2022YFS0634) and Central Guidance for Local Scientific and Technological Development Projects (grant no. 2023ZYD0112).

Availability of data and materials

The data generated in the present study may be requested from the corresponding author. The RNA sequencing data generated in the present study may be found in the GEO database under accession number GSE266150 or at the following URL: https://www.ncbi.nlm.nih.gov/geo/query/acc.cgi?&acc=GSE266150.

Authors' contributions

SL and XX conceived and designed the experiments. ZX, YL, QZ and LZ performed the experiments, prepared the manuscript and analyzed the data. SL and XX confirm the authenticity of all the raw data. All authors have read and approved the final version of the manuscript.

Ethics approval and consent to participate

The isolation of hPDLSCs from patient samples was approved by the Ethics Committee of The Affiliated Stomatology Hospital, Southwest Medical University (Luzhou, China; approval no. 20221107003). Written consent was provided by the guardians and patients for the use of samples in the present research project. The animal experiments followed the guidelines of the National Institutes of Health and were approved by the Ethics Committee of the Laboratory Animal Center of Southwest Medical University (Luzhou, China; approval no. 20221107-016).

Patient consent for publication

Not applicable.

Competing interests

The authors declare that they have no competing interests.

References

1. Alves LS, Aragão I, Sousa MJC and Gomes E: Pattern of maxillofacial fractures in severe multiple trauma patients: A 7-year prospective study. Braz Dent J 25: 561-564, 2014.
2. Reddi AH: Symbiosis of biotechnology and biomaterials: Applications in tissue engineering of bone and cartilage. J Cell Biochem 56: 192-195, 1994.
3. Li J, Wang Z, Huang X, Wang Z, Chen Z, Wang R, Chen Z, Liu W, Wu B, Fang F and Qiu W: Dynamic proteomic profiling of human periodontal ligament stem cells during osteogenic differentiation. Stem Cell Res Ther 12: 98, 2021.
4. Huang GTJ, Gronthos S and Shi S: Mesenchymal stem cells derived from dental tissues vs those from other sources: Their biology and role in regenerative medicine. J Dent Res 88: 792-806, 2009.
5. Hwang NS, Zhang C, Hwang YS and Varghese S: Mesenchymal stem cell differentiation and roles in regenerative medicine. Wiley Interdiscip Rev Syst Biol Med 1: 97-106, 2009.
6. Chen HJ, Inbaraj BS and Chen BH: Determination of phenolic acids and flavonoids in Taraxacum formosanum Kitam by liquid chromatography-tandem mass spectrometry coupled with a post-column derivatization technique. Int J Mol Sci 13: 260-285, 2012.
7. Shi Y, Dai J, Liu H, Li RR, Sun PL, Du Q, Pang LL, Chen Z and Yin KS: Naringenin inhibits allergen-induced airway inflammation and airway responsiveness and inhibits NF-kappaB activity in a murine model of asthma. Can J Physiol Pharmacol 87: 729-735, 2009.
8. Renugadevi J and Prabu SM: Naringenin protects against cadmium-induced oxidative renal dysfunction in rats. Toxicology 256: 128-134, 2009.
9. Uçar K and Göktaş Z: Biological activities of naringenin: A narrative review based on in vitro and in vivo studies. Nutr Res 119: 43-55, 2023.
10. Kaczmarczyk-Sedlak I, Wojnar W, Zych M, Ozimina-Kamińska E and Bońka A: Effect of dietary flavonoid naringenin on bones in rats with ovariectomy-induced osteoporosis. Acta Pol Pharm 73: 1073-1081, 2016.
11. Gera S, Sampathi S, Maddukuri S, Dodoala S, Junnuthula V and Dyawanapelly S: Therapeutic potential of naringenin nanosuspension: In vitro and in vivo anti-osteoporotic studies. Pharmaceutics 14: 1449, 2022.
12. Zhang L, He H, Zhang M, Wu Y, Xu X, Yang M and Mei L: Assessing the effect and related mechanism of naringenin on the proliferation, osteogenic differentiation and endothelial differentiation of human periodontal ligament stem cells. Biochem Biophys Res Commun 534: 337-342, 2021.
13. Wu Z, Li W, Liu G and Tang Y: Network-based methods for prediction of drug-target interactions. Front Pharmacol 9: 1134, 2018.
14. Dorado G, Gálvez S, Rosales TE, Vásquez VF and Hernández P: Analyzing modern biomolecules: The revolution of nucleic-acid sequencing-review. Biomolecules 11: 1111, 2021.
15. Li S, Fan TP, Jia W, Lu A and Zhang W: Network pharmacology in traditional chinese medicine. Evid Based Complement Alternat Med 2014: 138460, 2014.
16. Zhang R, Zhu X, Bai H and Ning K: Network pharmacology databases for traditional Chinese medicine: Front Pharmacol 10: 123, 2019.
17. Livak KJ and Schmittgen TD: Analysis of relative gene expression data using real-time quantitative PCR and the 2(-Delta Delta C(T)) method. Methods 25: 402-408, 2001.
18. Morris GM, Huey R, Lindstrom W, Sanner MF, Belew RK, Goodsell DS and Olson AJ: AutoDock4 and AutoDockTools4: Automated docking with selective receptor flexibility. J Comput Chem 30: 2785-2791, 2009.
19. Morris GM, Huey R and Olson AJ: Using AutoDock for ligand-receptor docking. Curr Protoc Bioinformatics Chapter 8: Unit 8.14, 2008.
20. Xu HY, Zhang YQ, Liu ZM, Chen T, Lv CY, Tang SH, Zhang XB, Zhang W, Li ZY, Zhou RR, *et al*: ETCM: An encyclopaedia of traditional Chinese medicine. Nucleic Acids Res 47 (D1): D976-D982, 2019.
21. Rahigude A, Bhutada P, Kaulaskar S, Aswar M and Otari K: Participation of antioxidant and cholinergic system in protective effect of naringenin against type-2 diabetes-induced memory dysfunction in rats. Neuroscience 226: 62-72, 2012.
22. Renugadevi J and Prabu SM: Cadmium-induced hepatotoxicity in rats and the protective effect of naringenin. Exp Toxicol Pathol 62: 171-181, 2010.
23. AVMA Panel on Euthanasia. American Veterinary Medical Association: 2000 report of the AVMA panel on euthanasia. J Am Vet Med Assoc 218: 669-696, 2001.
24. Ren S, Zhou Y, Zheng K, Xu X, Yang J, Wang X, Miao L, Wei H and Xu Y: Cerium oxide nanoparticles loaded nanofibrous membranes promote bone regeneration for periodontal tissue engineering. Bioact Mater 7: 242-253, 2021.
25. Lai S, Liu C, Liu C, Fan L, Li X, Yang Y, Zhu Y, Deng L, Xiao L and Mu Y: Lycium barbarum polysaccharide-glycoprotein promotes osteogenesis in hPDLSCs via ERK activation. Oral Dis 29: 3503-3513, 2023.

26. Li N, Li Z, Wang Y, Chen Y, Ge X, Lu J, Bian M, Wu J and Yu J: CTP-CM enhances osteogenic differentiation of hPDLSCs via NF-κB pathway. Oral Dis 27: 577-588, 2021.
27. Kim SM, Yuen T, Iqbal J, Rubin MR and Zaidi M: The NO-cGMP-PKG pathway in skeletal remodeling. Ann N Y Acad Sci 1487: 21-30, 2021.
28. Joshua J, Kalyanaraman H, Marathe N and Pilz RB: Nitric oxide as a mediator of estrogen effects in osteocytes. Vitam Horm 96: 247-263, 2014.
29. Liu L, Yuan W and Wang J: Mechanisms for osteogenic differentiation of human mesenchymal stem cells induced by fluid shear stress. Biomech Model Mechanobiol 9: 659-670, 2010.
30. Zhai YK, Guo XY, Ge BF, Zhen P, Ma XN, Zhou J, Ma HP, Xian CJ and Chen KM: Icariin stimulates the osteogenic differentiation of rat bone marrow stromal cells via activating the PI3K-AKT-eNOS-NO-cGMP-PKG. Bone 66: 189-198, 2014.
31. Yan T, Xie Y, He H, Fan W and Huang F: Role of nitric oxide in orthodontic tooth movement (review). Int J Mol Med 48: 168, 2021.
32. Kalyanaraman H, Ramdani G, Joshua J, Schall N, Boss GR, Cory E, Sah RL, Casteel DE and Pilz RB: A novel, direct no donor regulates osteoblast and osteoclast functions and increases bone mass in ovariectomized mice. J Bone Miner Res 32: 46-59, 2017.
33. Joshua J, Schwaerzer GK, Kalyanaraman H, Cory E, Sah RL, Li M, Vaida F, Boss GR and Pilz RB: Soluble guanylate cyclase as a novel treatment target for osteoporosis. Endocrinology 155: 4720-4730, 2014.
34. Wang L, Mi J, Sun B, Yang G, Liu S, Chen M, Yu L, Pan J and Liu Y: Role of transient receptor potential channel 6 in the osteogenesis of periodontal ligament cells. Int Immunopharmacol 100: 108134, 2021.
35. Cai Z, Wu C, Xu Y, Cai J, Zhao M and Zu L: The NO-cGMP-PKG axis in HFpEF: From pathological mechanisms to potential therapies. Aging Dis 14: 46-62, 2023.
36. Lu M, Wang Y, Jiang Y, Zhang C, Wang H, Sha W, Chen L, Lei T and Liu L: Berberine inhibits gluconeogenesis in spontaneous diabetic rats by regulating the AKT/MAPK/NO/cGMP/PKG signaling pathway. Mol Cell Biochem 478: 2013-2027, 2023.
37. Plano SA, Alessandro MS, Trebucq LL, Endo S, Golombek DA and Chiesa JJ: Role of G-substrate in the NO/cGMP/PKG signal transduction pathway for photic entrainment of the hamster circadian clock. ASN Neuro 13: 1759091420984920, 2021.
38. Manchope MF, Calixto-Campos C, Coelho-Silva L, Zarpelon AC, Pinho-Ribeiro FA, Georgetti SR, Baracat MM, Casagrande R and Verri WA Jr: Naringenin inhibits superoxide anion-induced inflammatory pain: Role of oxidative stress, cytokines, Nrf-2 and the NO-cGMP-PKG-KATP channel signaling pathway. PLoS One 11: e0153015, 2016.
39. Kim HJ and Kim BJ: Naringenin inhibits pacemaking activity in interstitial cells of Cajal from murine small intestine. Integr Med Res 6: 149-155, 2017.
40. Lin H, Wang X, Liu M, Huang M, Shen Z, Feng J, Yang H, Li Z, Gao J and Ye X: Exploring the treatment of COVID-19 with Yinqiao powder based on network pharmacology. Phytother Res 35: 2651-2664, 2021.
41. Qu Y, Yang X, Li J, Zhang S, Li S, Wang M, Zhou L, Wang Z, Lin Z, Yin Y, *et al*: Network pharmacology and molecular docking study of Zhishi-Baizhu Herb Pair in the treatment of gastric cancer. Evid Based Complement Alternat Med 2021: 2311486, 2021.
42. Yao T, Wang Q, Han S, Lu Y, Xu Y and Wang Y: Potential molecular mechanisms of ephedra herb in the treatment of nephrotic syndrome based on network pharmacology and molecular docking. Biomed Res Int 2022: 9214589, 2022.
43. Duan MX, Zhou H, Wu QQ, Liu C, Xiao Y, Deng W and Tang QZ: Andrographolide protects against HG-induced inflammation, apoptosis, migration, and impairment of angiogenesis via PI3K/AKT-eNOS signalling in HUVECs. Mediators Inflamm 2019: 6168340, 2019.
44. Jo H, Mondal S, Tan D, Nagata E, Takizawa S, Sharma AK, Hou Q, Shanmugasundaram K, Prasad A, Tung JK, *et al*: Small molecule-induced cytosolic activation of protein kinase Akt rescues ischemia-elicited neuronal death. Proc Natl Acad Sci USA 109: 10581-10586, 2012.
45. Zhu R, Chen YX, Ke QF, Gao YS and Guo YP: SC79-loaded ZSM-5/chitosan porous scaffolds with enhanced stem cell osteogenic differentiation and bone regeneration. J Mater Chem B 5: 5009-5018, 2017.
46. Lim W, Park S, Bazer FW and Song G: Naringenin-induced apoptotic cell death in prostate cancer cells is mediated via the PI3K/AKT and MAPK signaling pathways. J Cell Biochem 118: 1118-1131, 2017.
47. Xu X, Lei T, Li W and Ou H: Enhanced cellular cholesterol efflux by naringenin is mediated through inhibiting endoplasmic reticulum stress-ATF6 activity in macrophages. Biochim Biophys Acta Mol Cell Biol Lipids 1864: 1472-1482, 2019.
48. Rashid R, Tripathi R, Singh A, Sarkar S, Kawale A, Bader GN, Gupta S, Gupta RK and Jha RK: Naringenin improves ovarian health by reducing the serum androgen and eliminating follicular cysts in letrozole-induced polycystic ovary syndrome in the Sprague Dawley rats. Phytother Res 37: 4018-4041, 2023.
49. Lim W and Song G: Naringenin-induced migration of embrynoic trophectoderm cells is mediated via PI3K/AKT and ERK1/2 MAPK signaling cascades. Mol Cell Endocrinol 428: 28-37, 2016.
50. Zhou X, Zhang Z, Jiang W, Hu M, Meng Y, Li W, Zhou X and Wang C: Naringenin is a potential anabolic treatment for bone loss by modulating osteogenesis, osteoclastogenesis, and macrophage polarization. Front Pharmacol 13: 872188, 2022.
51. Hombach S and Kretz M: Non-coding RNAs: Classification, biology and functioning. Adv Exp Med Biol 937: 3-17, 2016.